Available online at www.sciencedirect.com
ScienceDirect
International Journal of Heat and Mass Transfer 51 (2008) 1216–1225
International Journal of HEAT and MASS TRANSFER
www.elsevier.com/locate/ijhmt

A theoretical model for the prediction of the critical heat flux in heated microchannels

Rémi Revellin, John R. Thome *

Ecole Polytechnique Fédérale de Lausanne, STI ISE LTCM, ME G1 464, Station 9, CH-1015 Lausanne, Switzerland

Received 3 August 2006; received in revised form 1 March 2007
Available online 27 April 2007

Abstract

A theoretical model for the prediction of the critical heat flux of refrigerants flowing in heated, round microchannels has been developed and presented here. The model is based on the two-phase conservation equations and includes the effect of the height of the interfacial waves of the annular film. Validation has been carried out by comparing the model, a numerical solution of a non-linear system of five differential equations, with a critical heat flux (CHF) database including three different refrigerants from two different laboratories. More than 96% of the data are predicted within a ±20% error band and a mean absolute error of 8%. Furthermore, it is also possible to predict CHF data from a third laboratory for water and R-113 flowing in rectangular (using the width of the channel as the characteristic dimension) and circular microchannel heat sinks with multiple channels. All together, 90% of the entire database, including four different fluids and different geometries, are predicted by the model within a ±20% error band and a mean absolute error of 9.3% for channels from 0.215 to 3.15 mm in size, mass fluxes from 29 to 1600 kg/m^2 s, heated lengths from 10 to 126 mm and subcoolings from 2 to 77 °C.

Keywords: Microchannel; CHF; Annular flow; Interfacial waves

1. Introduction

Critical heat flux (CHF) or burnout is a limiting operating heat flux for the safe operation of heat dissipation applications and refers to the replacement of liquid being in contact with the heated surface with a vapor blanket, a phenomenon similar to that occuring in macroscale CHF. The thermal conductivity of the vapor is very low compared to the liquid and the surface heat transfer coefficient drops dramatically, resulting in the sudden increase of the surface temperature and possible failure of the cooled device. CHF may occur in subcooled as well as in saturated boiling conditions. In subcooled CHF, the bulk temperature at the channel outlet is subcooled and the thermodynamic equilibrium vapor quality is lower than zero, $x < 0$. These are the typical conditions for very high mass velocities, high inlet subcoolings and relative short channels compared to their hydraulic diameters. In saturated CHF, the thermodynamic equilibrium vapor quality at the channel outlet is greater or equal to zero, $x \geqslant 0$. This is typically encountered at low mass velocities, at low inlet subcoolings and in channels with a large length to diameter ratio. Before the use of microchannels under saturated boiling conditions becomes widely used as a cooling method of high heat flux devices such as computer CPU's, power electronics and laser diodes, it is essential to understand the CHF mechanism.

Bergles and Kandlikar [1] reviewed the existing studies on critical heat flux in microchannels. They concluded by saying that single-tube CHF data are not available for microchannels. For the case of parallel multichannels they noted that all the available CHF data were taken under unstable conditions. The critical condition is the result of an upstream compressible volume instability or the parallel channel, Ledinegg instability. As a result, the CHF values are lower than they would be if the channel flow were kept stable by an inlet restriction at the inlet of each channel.

* Corresponding author. Tel.: +41 21 693 5981; fax: +41 21 693 5960.
E-mail address: john.thome@epfl.ch (J.R. Thome).

0017-9310/$ - see front matter © 2007 Published by Elsevier Ltd.
doi:10.1016/j.ijheatmasstransfer.2007.03.002

Nomenclature

A	cross sectional area, m^2
B	empirical constant
C	empirical constant
C_f	fanning friction factor
CHF	critical heat flux, kW/m^2
dz	element of discretization, m
D	diameter, m
Δh_{in}	inlet enthalpy of subcooling, J/kg
g	acceleration of gravity, m/s^2
G	mass flux, kg/m^2 s
G_{wavy}	wavy flow transition mass flux, kg/m^2 s
h_{LV}	latent heat of vaporization, J/kg
j	exponent
j_1	exponent
k	exponent
k_1	exponent
K	empirical inlet subcooling parameter of Katto and Ohno
L	length, m
$\dot{m}$	mass flow, kg/s
$\dot{m}_e$	rate of evaporation, kg/s
MAE	mean absolute error $= \frac{1}{N}\sum_1^N \left\lvert \frac{\text{predicted value}-\text{experimental value}}{\text{experimental value}} \right\rvert \times 100$, %
p	pressure bar
P	perimeter of the tube, m
q	heat flux, kW/m^2
q_c	CHF for subcooled conditions, kW/m^2
q_{co}	saturated CHF of Katto and Ohno, kW/m^2
r	radius of the vapor core, m
R	internal radius of the tube, m
Re	Reynolds number
T	temperature, °C
u	velocity, m/s
We	Weber number
x	vapor quality
z	length along channel from entrance m

Greek symbols

Δ	difference
$\Delta\delta_i$	height of the interfacial waves, μm
δ	film thickness, μm
λ_c	one dimensional critical Kelvin–Helmholtz instability wavelength, m
μ	dynamic viscosity, Pa s
ρ	density, kg/m^3
σ	surface tension, N/m
τ	shear stress, N/m^2

Subscripts

h	heated
i	interfacial
L	liquid
min	minimum
O	only
sat	saturation
sub	subcooling
V	vapor
w	wall

One of the most widely used empirical methods developed for predicting saturated CHF in a single channel is the Katto and Ohno [2] correlation. For no liquid subcooling, they correlated CHF with q_{co} given as:

$$\frac{q_{co}}{Gh_{LV}} = f\left[\frac{\rho_L}{\rho_V}, \frac{\sigma\rho_L}{G^2L}, \frac{L}{D}\right] \quad (1)$$

For most regimes, they found a linear rise in CHF with increasing liquid subcooling. Therefore, subcooling was taken into account by the following equation:

$$\frac{q_c}{Gh_{LV}} = q_{co}\left(1 + K\frac{\Delta h_{in}}{h_{LV}}\right) \quad (2)$$

To ascertain the applicability of the above correlation to fluids other than water, they conducted the following experiments:

- R-12 for $D = 3.0$ and 5.0 mm, $L_h/D = 200$ and 333, $\rho_V/\rho_L = 0.109$–0.306 and $G = 1100$–8800 kg/m^2 s in Katto and Yokoya [3];
- R-12 for $D = 5.0$ mm, $L_h/D = 50$, $\rho_V/\rho_L = 0.109$–0.306 and $G = 700$–7000 kg/m^2 s in Katto and Ashida [4];
- liquid helium for $D = 1.0$ mm, $L_h/D = 25$–200, $\rho_V/\rho_L = 0.409$ and $G = 10.5$–108 kg/m^2 s in Katto and Yokoya [5].

Hence, for normal refrigerants this method is applicable only down to about 3.0 mm channels.

Qu and Mudawar [6] compared their 414 data points they obtained for water in channels with $D = 1.0$–3.0 mm and $L_h/D = 50$–975 and for R-113 with $D = 3.15$ mm and $L_h/D = 40$ to the correlation of Katto–Ohno. They found that this correlation is fairly accurate at predicting saturated CHF in single circular mini-channels. The mean absolute error for this correlation was 17.3% with most of the data points falling within a ±40% error band.

Furthermore, Qu and Mudawar [6] adapted the Katto–Ohno correlation for microchannel heat sinks containing 21 parallel 215 × 821 μm channels. They found that as CHF was approached, flow instabilities induced vapor backflow into the heat sink's upstream plenum, resulting in mixing vapor with subcooled liquid. The backflow negated the advantages of inlet subcooling, resulting in a CHF virtually independent of inlet subcooling. Their new empirical correlation based on their experimental CHF

data for water and R-113 (Bowers and Mudawar [7]) in mini/microchannel heat sinks is as follows:

$$\frac{q_c}{Gh_{LV}} = 33.43\left(\frac{\rho_V}{\rho_L}\right)^{1.11} We_{LO}^{-0.21}\left(\frac{L}{D}\right)^{-0.36} \quad (3)$$

with

$$We_{LO} = \frac{G^2 L}{\rho_L \sigma} \quad (4)$$

This correlation predicted their experimental data with very low mean absolute error of 4%.

Wojtan et al. [8] performed a series of tests to determine the CHF in 0.509 mm and 0.790 mm internal diameter microchannel tubes as a function of refrigerant mass velocity, heated length, saturation temperature and inlet liquid subcooling. The refrigerants tested were R-134a and R-245fa and the heated length of microchannel was varied from 20 and 70 mm. The results showed a strong dependence of CHF on mass velocity, heated length and microchannel diameter but no measurable influence of liquid subcooling (2–15 °C) was observed. The experimental results were compared to the CHF single-channel correlation of Katto and Ohno [2] and the multichannel correlation of Qu and Mudawar [6], showing that the correlation of Katto–Ohno predicted their microchannel data better with a mean absolute error of 32.8% with only 41.2% of the data falling within a ±15% error band. The correlation of Qu and Mudawar exhibited the same trends as the CHF data but significantly overpredicted them. Based on their experimental data, a new microscale version of the Katto–Ohno correlation for the prediction of CHF during saturated boiling in microchannels was proposed by Wojtan et al.:

$$\frac{q_c}{Gh_{LV}} = 0.437\left(\frac{\rho_V}{\rho_L}\right)^{0.073} We_{LO}^{-0.24}\left(\frac{L}{D}\right)^{-0.72} \quad (5)$$

with

$$We_{LO} = \frac{G^2 L}{\sigma \rho_L} \quad (6)$$

Wojtan et al. [8] observed the occurrence of dryout in the annular flow regime. This characteristic was also reported by Revellin et al. [9]. Through an energy balance based on the CHF correlation, they calculated the critical vapor quality. In a mass flux versus vapor quality diabatic flow pattern map, they reported the annular-to-dryout transition. Beyond this limit mist flow occurs.

Pribyl et al. [10] studied the effect of the flow patterns on CHF. They plotted experimental water CHF data obtained in three independent test facilities against vapor quality. The total number of experimental points was 4109. The tube diameters tested varied from 1.0 to 37.0 mm, heated lengths from 31 to 3000 mm and mass flux from 10 to 18580 kg/m^2 s. The database was sorted by regime using the Taitel and Dukler [11] map to identify annular, intermittent and bubble flows. They found that CHF varied linearly with quality in distinct segments, with a relatively sharp discontinuity and change in slope at low vapor qualities, where the Taitel–Dukler map predicts a regime transition. The most apparent difference in slope was observed between bubble and annular flow. They concluded that a change in flow regime might affect the mechanism of CHF and that within each flow regime a similar but distinct CHF mechanism could be expected to apply.

Wojtan et al. [12] investigated flow boiling in horizontal tubes. Annular-to-dryout and dryout-to-mist flow transition curves have been added and integrated into their new macroscale diabatic flow pattern map, identified by distinct trends of the heat transfer coefficient as a function of vapor quality and by flow pattern observations to determine (and then predict) the inception and completion of dryout in horizontal tubes. The distinction of these two points is caused by the shift of the dryout position from the top to the bottom around and along the tube perimeter with increasing quality and also by the irregular fluctuations of the axial dryout position due to the unstable nature of the process. However, in small channels, we can assume a nearly uniform circumferential distribution of the liquid film, so that dryout occurs simultaneously all around the perimeter.

Critical heat flux is an important parameter for the safe operation of heat sinks operating at high heat fluxes. Developing a theoretical model rather than resorting to a correlation for predicting CHF should yield a more general method based on the physical phenomenon causing dryout. Here, a model for the prediction of the critical heat flux in circular tubes has been developed, based on a non-linear system of five differential equations and then extended to non-circular channels.

2. Description of the model

2.1. Principle

Many experimental observations confirm that the critical heat flux (CHF) in microchannels occurs in annular flow, such as has been observed in Wojtan et al. [8] and Revellin and Thome [13]. For this reason, a theoretical model based on the dryout of the liquid film during evaporation in annular flow has been developed for refrigerants flowing at stable conditions in uniformly heated, circular microchannels. Dryout occurs when the liquid film ($\delta = 0$) has been exhausted. In this situation, the vapor is then in contact with the tube wall and the heat transfer coefficient falls sharply and the wall temperature jumps rapidly. For annular flows in microchannels without interfacial waves, this is the case at low mass fluxes and for the vapor quality x equal to 1.

Another mechanism of dryout is vapor shear overcoming surface tension forces to remove the liquid film from the wall, i.e. the G_{wavy} boundary. This film dryout phenom-

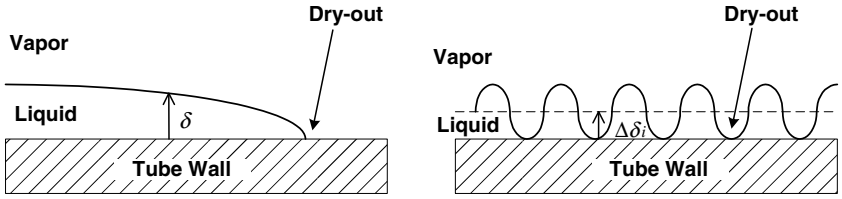

Fig. 1. Film thickness when dryout occurs. Left: without interfacial waves. Right: with interfacial waves.

enon occurs when the average liquid film is still greater than 0 ($\delta > 0$) if the interfacial waves are large enough to have their trough in contact with the wall as shown in Fig. 1. In this situation, $x < 1$. It is assumed here that dry-out at high heat flux by this mechanism occurs first because the G_{wavy} boundary is for very high vapor quality. Based on the high speed, high definition videos taken in Revellin [14], we also observed that there appears to be little liquid entrained in the gas core. Here, a new hydrodynamic model is proposed that takes into account the conservation of mass and momentum, an energy balance with the wall (any potentially significant axial or radial conduction effects in the wall are neglected here) and the height of the interfacial waves ($\Delta\delta_i$), in a one dimensional finite volume model.

Fig. 2 shows the control volume of the model where $R = \delta + r$ and $\tau_{LV} = -\tau_{LV}$. The shear stresses are determined using the conventional analytical relation for laminar flow in a tube and the well-known empirical relations for turbulent flow (Eq. (7)). The mass flux G is that of the liquid and vapor flowing through the cross section of the microchannel. The expressions used are as follows:

$$\tau_{LV} = \frac{1}{2} C_f \rho_V u_V^2 \text{ where}$$
$$C_f = \frac{16}{Re_V} \text{ for } Re_V = \frac{2\rho_V u_V r}{\mu_V} < 2300 \quad (7)$$
$$C_f = 0.078 Re_V^{-0.25} \text{ for } Re_V \geqslant 2300$$

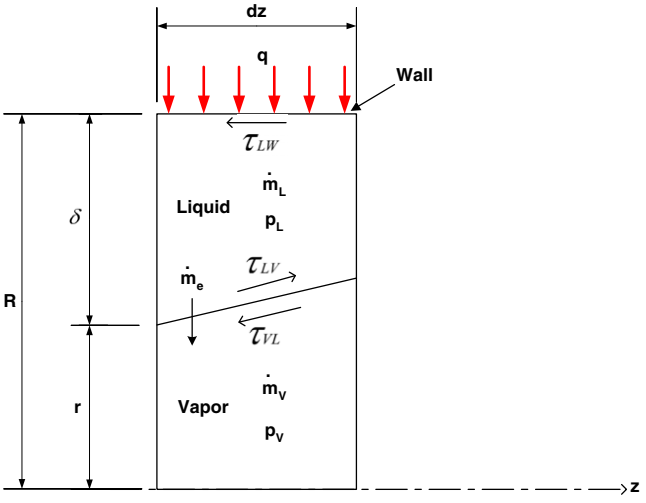

Fig. 2. Control volume of the model.

From conservation of mass and an energy balance assuming a separated flow model, we obtain the first two equations:

$$\frac{d(A_L u_L)}{dz} dz = -\frac{qP}{h_{LV}\rho_L} dz \quad (8)$$
$$\frac{d(A_V u_V)}{dz} dz = \frac{qP}{h_{LV}\rho_V} dz \quad (9)$$

where $A_L = \pi(R^2 - r^2)$ and $A_V = \pi r^2$ are the cross sections of the channel occupied by the liquid and the vapor, u_L and u_V are the mean velocities of each phase and $P = 2\pi R$ is the internal perimeter of the tube.

The conservation of momentum gives two additional equations:

$$\rho_L \frac{d(A_L u_L^2)}{dz} dz = -A_L \frac{dp_L}{dz} dz + A_i|\tau_{LV}| - A_{LW}|\tau_{LW}| \quad (10)$$
$$\rho_V \frac{d(A_V u_V^2)}{dz} dz = -A_V \frac{dp_V}{dz} dz - A_i|\tau_{VL}| \quad (11)$$

where $A_i = \sqrt{2}\pi(2r + dz)dz$ is the liquid/vapor interfacial area, $A_{LW} = 2\pi R dz$ is the liquid/wall interfacial area and A_i, A_L and A_V are only functions of r. τ_{LW} is the liquid/wall shear stress expressed by Eq. (12):

$$\tau_{LW} = \frac{1}{2} C_f \rho_L u_L^2 \text{ where}$$
$$C_f = \frac{16}{Re_L} \text{ for } Re_L = \frac{2\rho_L u_L (R - r)}{\mu_L} < 2300 \quad (12)$$
$$C_f = 0.078 Re_L^{-0.25} \text{ for } Re_L \geqslant 2300$$

To close the system, the Laplace–Young equation is used:

$$\frac{dp_V}{dz} - \frac{dp_L}{dz} = \frac{d}{dz}\left(\frac{\sigma}{r}\right) \quad (13)$$

2.2. The boundary conditions

We thus obtain a first order, non-linear system of five ordinary differential equations with five unknowns: r, u_V, u_L, p_V and p_L. The flow at the inlet at $z = 0$ is assumed to be saturated liquid. The system is numerically solved using the fourth order Runge–Kutta method with the following boundary conditions:

$$
\begin{aligned}
r|_{z=0} &= r_{\min} \\
u_V|_{z=0} &= \frac{G}{\rho_L} \\
u_L|_{z=0} &= \frac{G}{\rho_L} \\
p_V|_{z=0} &= p_{sat} \\
p_L|_{z=0} &= p_{sat} - \frac{\sigma}{r_{\min}}
\end{aligned}
\tag{14}
$$

$r_{\min}$ is theoretically equal to 0 at $z = 0$ but numerically has been set to $r_{\min} \simeq 0.1R$. There is only a minor effect of the choice of the value of $r_{\min}$ on the final CHF results. As an example for R-134a, $G = 500\ \text{kg/m}^2\,\text{s}$, $L = 70\ \text{mm}$, $T_{sat} = 30\ ^\circ\text{C}$ and $\Delta T_{sub} = 0\ ^\circ\text{C}$, $\text{CHF} = 123\ \text{kW/m}^2$ for $r_{\min} = 0.1R$. Furthermore, $\text{CHF} = 127\ \text{kW/m}^2$ for $r_{\min} = 0.3R$ and $\text{CHF} = 120\ \text{kW/m}^2$ for $r_{\min} = 0.03R$. Thus, there is a variation of less than 6% on CHF for $r_{\min}$ multiplied by a factor of 10. Here, $r_{\min} \simeq 0.1R$ has been chosen as an intermediate value to use in the implementation of the method.

2.3. The interfacial waves

For a given length and flow rate, the heat flux q can be determined in order to obtain dryout conditions at the outlet of the tube. As shown in Fig. 1, if there are no interfacial waves, dryout occurs when $x = 1$ and thus $\delta = 0$. If there are interfacial waves, dryout occurs when $\delta > 0$ and $x < 1$, where x is the thermodynamic vapor quality. Here, the model assumes no entrainment. The program stops when the calculated liquid film thickness is equal to the height of the interfacial waves, thus when $\Delta\delta_i = \delta$. The method proposed for predicting the height of the interfacial waves in an annular flow in a microchannel is given below.

Based on the theory of the interfacial roughness for condensation in horizontal tubes in Thome et al. [15], the height of the interfacial waves can be expected to be a function of the interfacial shear τ_i, where τ_i in turn depends on the velocity difference between the two phases, $(u_V - u_L)$. Since normally $u_V \gg u_L$, then $(u_V - u_L) \simeq u_V$. If we normalize the vapor velocity with that of the liquid, we get the slip ratio, u_V/u_L, typical of void fraction models. Thus, the height of the interfacial waves $\Delta\delta_i$ can be assumed to be proportional to $(u_V/u_L)^j$ where the exponent j is unknown. In addition, the Kelvin–Helmholtz instability mechanism is important in wave-propagation phenomena, particularly for flows in a confined channel (Kordyban [16]). The one dimensional Kelvin–Helmholtz critical wavelength λ_c for a liquid film trapped between the vapor core and the tube is

$$
\lambda_c \left[\frac{(\rho_L - \rho_V)g}{\sigma}\right]^{1/2} = 2\pi \tag{15}
$$

This wave length should also be related to the formation of interfacial waves. If the interfacial waves have characteristic wavelengths proportional to the film thickness (this seems likely in very thin films because of the limited supply of liquid available to make the waves), then substituting $B\delta$ for λ_c means that the height of the interfacial waves $\Delta\delta_i$ will be approximately scaled as

$$
\Delta\delta_i \propto \left[\frac{(\rho_L - \rho_V)g(B\delta)^2}{\sigma}\right]^k \tag{16}
$$

where the term inside the brackets is non-dimensional. Based on this reasoning, the height of the interfacial waves is

$$
\frac{\Delta\delta_i}{R} = \left(\frac{u_V}{u_L}\right)^j \left(\frac{(\rho_L - \rho_V)g(B\delta)^2}{\sigma}\right)^k \tag{17}
$$

Critical heat flux occurs when $\delta = \Delta\delta_i$ i.e.

$$
\delta = B^{\frac{2k}{1-2k}} R \left(\frac{u_V}{u_L}\right)^{\frac{j}{1-2k}} \left(\frac{(\rho_L - \rho_V)gR^2}{\sigma}\right)^{\frac{k}{1-2k}} \tag{18}
$$

or

$$
\delta = CR \left(\frac{u_V}{u_L}\right)^{j_1} \left(\frac{(\rho_L - \rho_V)gR^2}{\sigma}\right)^{k_1} \tag{19}
$$

Expression (19) was adjusted using the experimental data of Wojtan et al. [8] and Lazareck and Black [17] to reach the dryout condition at the outlet of the tube. Based on the test data, the best value of the parameter C was found to be 0.15 and the exponents j_1 and k_1 to have nominal values of $-3/7$ and $-1/7$. The program stops when Eq. (19) is satisfied at the outlet of the microchannel. The liquid and vapor Reynolds numbers Re_L and Re_V were laminar and turbulent at these test conditions, respectively. As can be seen in Eq. (19), the gravity g is taken into account. Stratified flows are not normally observed is horizontal microchannels (all of the present database is for horizontal channels) but that does not mean that g has no effect. There is a competition between the gravity, surface tension and vapor shear forces on the annular film, which creates interfacial waves that are visible in videos described in Revellin et al. [9] and in other studies. The use of the Kelvin–Helmholtz critical wavelength is thus a plausible starting point for such analysis. However, the presence of Kelvin–Helmholtz instabilities occurring in such films should be verified experimentally.

The inlet subcooling is taken into account using a heat balance and removing the single-phase heating length at each heat flux increment. The flow regime is assumed to always be annular along the channel. In the correlations of Katto and Ohno [2], Qu and Mudawar [6] and Wojtan et al. [8] the L/D ratio plays an important role whereas in Eq. (19) it does not because the geometry effect is directly taken into account in the model by the energy balance of the enthalpy absorbed by the evaporating fluid along the channel. The other advantage of this model is that a non-uniform heat flux can be applied for the calculation of the CHF, which is not the case with the above correlations. As the tube length is discretized, an integrated heat flux along the tube can be used.

The calculation starts at $x = 0$ with the initial conditions given by Eq. (14) and an assumed heat flux. Then one calculate the five parameters (r, u_V, u_L, p_V and p_L) for each increment along the tube. Depending on the equality of Eq. (19) at the outlet of the tube, the heat flux is increased or decreased and a new calculation is performed. The program stops when Eq. (19) is satisfied at the outlet of the microchannel.

3. Comparison with experimental data

The model has been tested with the data of Wojtan et al. [8] for R-245fa and R-134a and the data of Lazareck and Black [17] for R-113 for circular channels (Fig. 3). More than 96% of the data are predicted within a ±20% error band and a mean absolute error (MAE) of 8%. These results are very good and the comparison takes into account three different fluids, three tube diameters and the different experimental conditions summarized in Table 1. It is interesting to emphasize that the inlet subcooling ranges from 2 to 77 °C in the experimental data. This is a large range of inlet subcooling and it is taken into account very well in the model. A broader comparison with more data would be beneficial. However, few CHF data are available in the literature for microchannels.

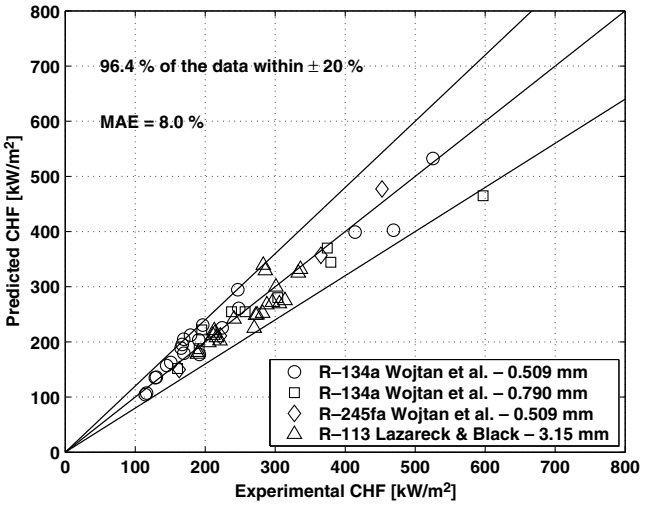

Fig. 3. Comparison between the model and the experimental data for circular tubes.

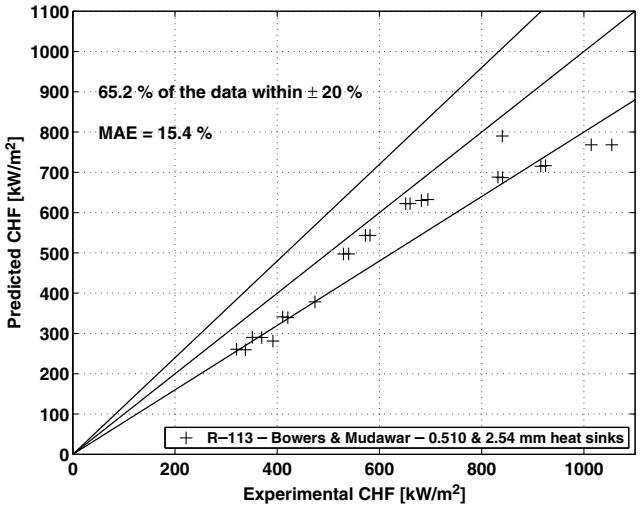

Fig. 4. Comparison between the model and the experimental data of Bowers and Mudawar [7] for R-113 in circular multi-microchannel heat sinks.

The data of Bowers and Mudawar [7] for R-113 flowing in mini and microchannel heat sinks have been digitized from their article. They studied CHF in 2.54 and 0.510 mm parallel circular channels of 10 mm heated length. Fig. 4 shows the comparison between the model and their experimental data, where 65.2% of the data are predicted within a ±20% error band and a mean absolute error of 15.4%. Here the deviation is a little larger because of the inaccuracy in digitizing the data from their graphs but it is still reasonable.

Qu and Mudawar [6] obtained critical heat flux data in microchannel heat sinks containing 21 parallel rectangular channels of 215 × 821 μm. Water was used as the test fluid. The rectangular microchannels were heated on only three sides. The diameter in the model was set to the width of the rectangular microchannels, i.e. $D = 0.215$ mm, to evaluate the model. This width is preferred to the hydraulic diameter as it seems to better take into account the confinement effect of the flow. The results are shown in Fig. 5, where 100% of the data are predicted within a ±20% error band and the mean absolute error is 5.5%. Obviously, instead of a circular tube, the geometry used in the model can be modified. This is the next future step of this work. However, it is possible to predict CHF in microchannel heat sinks with a very good accuracy by using the channel

Table 1
Experimental conditions

Study	Fluid	D (mm)	L (mm)	G (kg/m^2 s)	T_{sat} (°C)	ΔT_{sub} (°C)	CHF (kW/m^2)
Circular microchannel							
Wojtan et al. [8] (stainless steel)	R-134a R-245fa	0.509, 0.790	20–70.5	400–1600	30, 35	2–15	3.2–600
Lazareck and Black [17] (stainless steel)	R-113	3.15	126	232–503	48.4–98.3	2.16–74.41	183–336
Microchannel heat sinks							
Bowers and Mudawar [7] (copper and nickel)	R-113	0.510, 2.54	10	29–476.5	57.2	20	320–1055
Qu and Mudawar [6] (copper)	Water	0.215 × 0.821	44.73	85.9–368.4	105–109.2	45.16–77.1	264.2–542

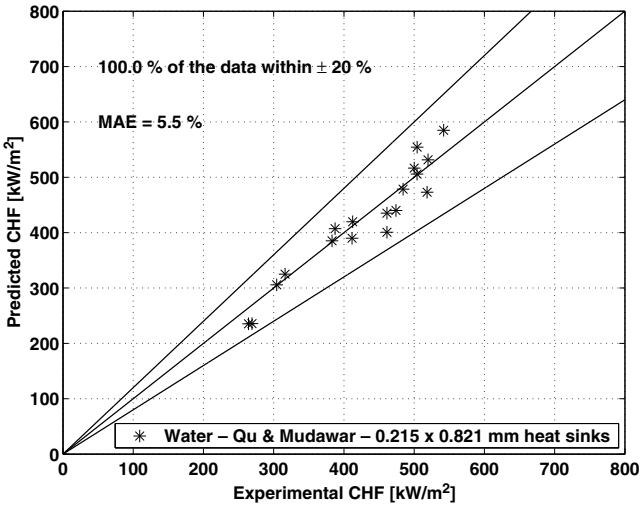

Fig. 5. Comparison between the model and the experimental data of Qu and Mudawar [6] for water in a rectangular multi-microchannel heat sink.

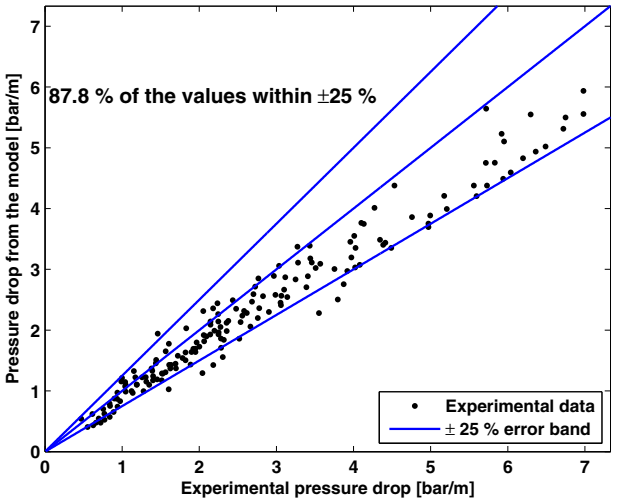

Fig. 7. Comparison between the adiabatic pressure drop from the model and the results of Revellin et al. [18] for smooth-annular flow for R-134a and R-245fa.

width as the characteristic dimension, at least for the present case.

Overall, 89.6% of the all database including the four different fluids and different geometries are predicted by the model within a ±20% error band (Fig. 6). The mean absolute error is 9.3% for the entire database. The database covers channels from 0.215 to 3.15 mm, mass velocities from 29 to 1600 kg/m^2 s, heated lengths from 10 to 126 mm and subcoolings from 2 to 77 °C.

In order to confirm that the model captures the mechanisms of smooth-annular flow, the adiabatic two-phase pressure drop measurements of Revellin et al. [18] in smooth annular flow have been compared with those calculated by the present model. The test section of Revellin et al. consisted of a microevaporator followed by an adiabatic glass tube were the pressure measurements were made. The model is implemented here of applying the experimental heat flux q to the microevaporator (the same as Revellin et al.) and adding a glass tube (the same length and diameter as Revellin et al.) after the microevaporator. The liquid film thickness, the velocities and pressures of each phase calculated at the exit of the microevaporator are applied at the inlet of the adiabatic glass tube. The adiabatic pressure drop calculation is then performed along the glass tube and compared with the Revellin et al. results. Fig. 7 shows a good agreement between the present numerical model and the experiments for smooth-annular flow for $D = 0.5$ mm and two fluids: R-134a and R-245fa. Almost 88% of the database are predicted within a ±25% error band. These results confirm that the model captures the hydrodynamics of smooth-annular flow in a microchannel.

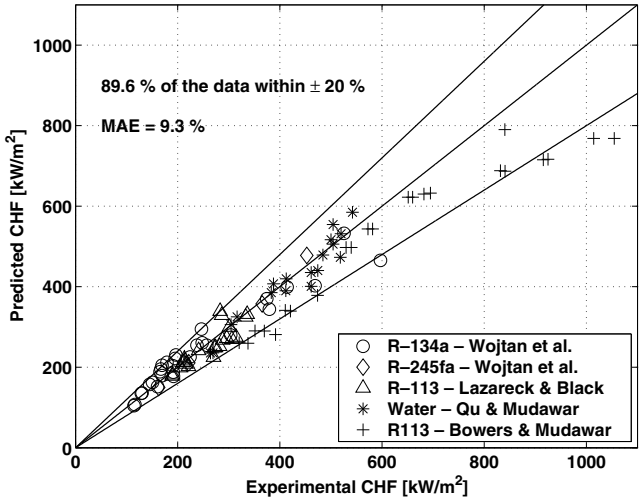

Fig. 6. Comparison between the model and the entire database.

4. Critical vapor quality

As shown in Wojtan et al. [8] and Revellin and Thome [13], the critical vapor quality defines the annular-to-dryout transition in a diabatic flow pattern map. Beyond this zone, damage from overheating can occur for the device being cooled by the microchannels, such as a microprocessor. The critical vapor quality is thus the upper operating limitation for the exit vapor quality of heat sinks, a representation that can be shown in a diabatic flow pattern map as in [13]. The critical vapor quality has been determined here using an energy balance as follows assuming a uniform heat flux along the channel:

$$x_{\text{crit}} = \frac{q_{\text{CHF}}}{Gh_{\text{LV}}}\frac{4L}{D} \tag{20}$$

A comparison between the experimental data for R-134a, the correlation of Wojtan et al. [8] and the new CHF model has been carried out. The results are shown

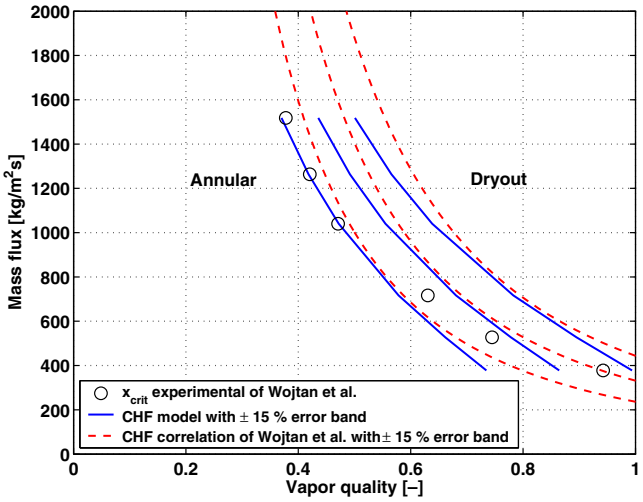

Fig. 8. Transition from annular flow to dryout for R-134a, $D = 0.509$ mm, $L_{MEV} = 70$ mm and $T_{sat} = 30$ °C.

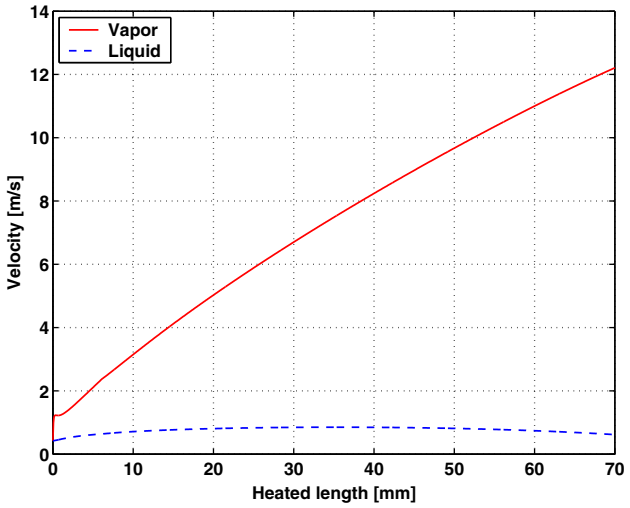

Fig. 10. Evolution of the liquid and vapor velocities along the microchannel for R-134a, $D = 0.5$ mm, $L = 70$ mm, $G = 500$ kg/m^2 s, $T_{sat} = 30$ °C, $\Delta T_{sub} = 0$ °C and $q = 123$ kW/m^2.

in Fig. 8. It is clearly observed that the new CHF model predicts the experimental data with a better accuracy than the correlation of Wojtan et al. [8].

5. Results and discussion

Fig. 9 shows the evolution of the annular liquid film thickness along a heated tube that decreases due to the evaporation process. The minimum film thickness here is $\delta = 17.4$ μm at the outlet of the tube and corresponds to the height of the interfacial waves when dryout occurs. The velocity of the liquid film increases along the tube as can be seen in Fig. 10 and decreases afterwards. It would reach $u_L = 0$ at the outlet of the tube at $x = 1$. The vapor velocity increases regularly along the tube. There is however a small change of slope at the beginning of the tube. This is due to the change of slope of the vapor pressure gradient as can be observed in Figs. 11 and 12. Besides that detail, the liquid and vapor pressures decrease along the tube, differing by the pressure drop across the vapor–liquid film as in Eq. (13).

The model is a system of five non-linear differential equations that is used together with the interfacial wave height prediction so an explicit expression of the critical heat flux is not defined. As a result, to determine the parametric sensitivities and dependencies, simulations have been run and are presented in different graphs that have been plotted.

Fig. 13 shows a simulation of the influence of the mass flux G and the diameter D on the critical heat flux calculated with the current model. As expected, the higher the mass flux, the higher the CHF. When the diameter

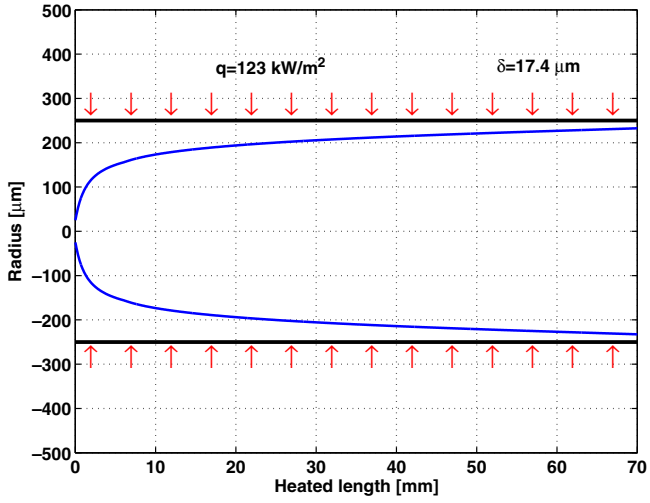

Fig. 9. Evolution of the liquid film thickness along the microchannel for R-134a, $D = 0.5$ mm, $L = 70$ mm, $G = 500$ kg/m^2 s, $T_{sat} = 30$ °C, $\Delta T_{sub} = 0$ °C and $q = 123$ kW/m^2.

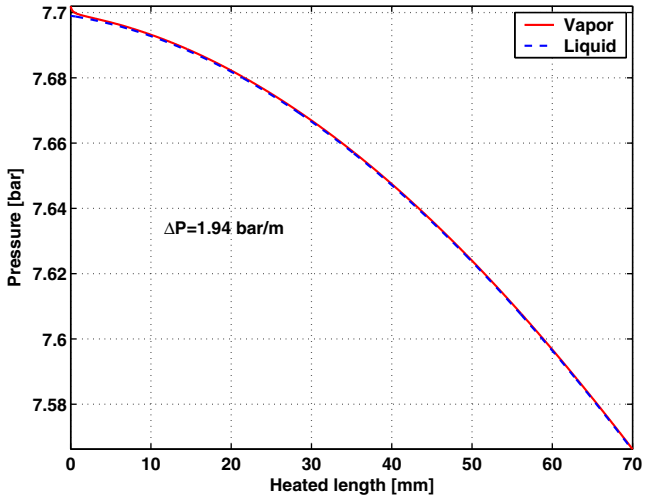

Fig. 11. Evolution of the liquid and vapor pressure along the microchannel for R-134a, $D = 0.5$ mm, $L = 70$ mm, $G = 500$ kg/m^2 s, $T_{sat} = 30$ °C, $\Delta T_{sub} = 0$ °C and $q = 123$ kW/m^2.

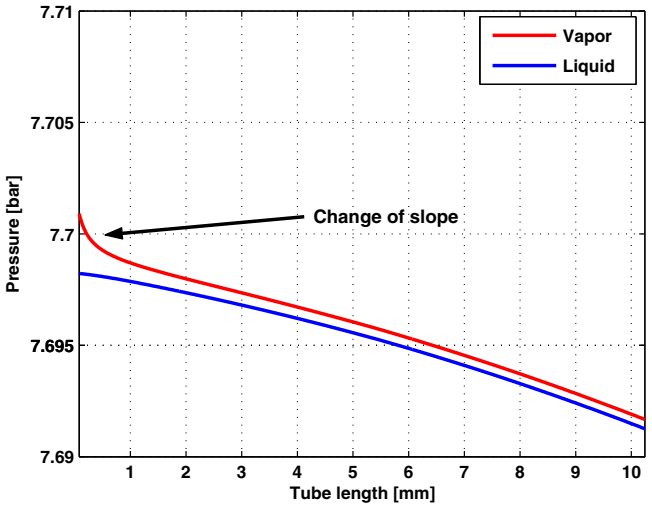

Fig. 12. Zoom on the evolution of the liquid and vapor pressure along the microchannel for R-134a, $D = 0.5$ mm, $L = 70$ mm, $G = 500$ kg/m^2 s, $T_{sat} = 30$ °C, $\Delta T_{sub} = 0$ °C and $q = 123$ kW/m^2.

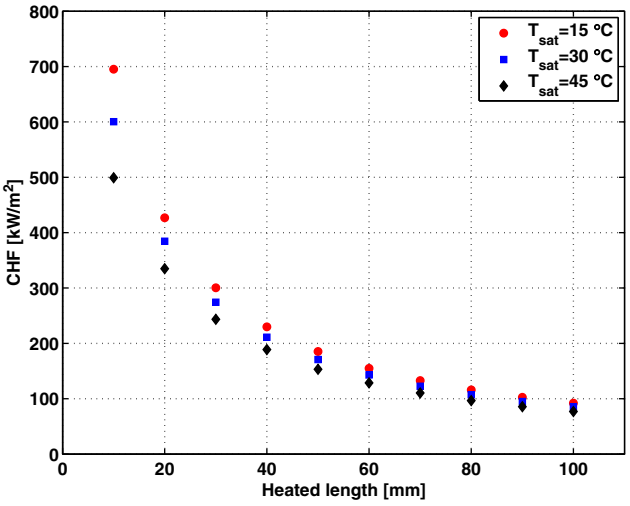

Fig. 14. Simulation of the influence of the heated length L and the saturation temperature T_{sat} on the critical heat flux calculated with the current model for R-134a, $D = 0.5$ mm, $G = 500$ kg/m^2 s and $\Delta T_{sub} = 0$ °C.

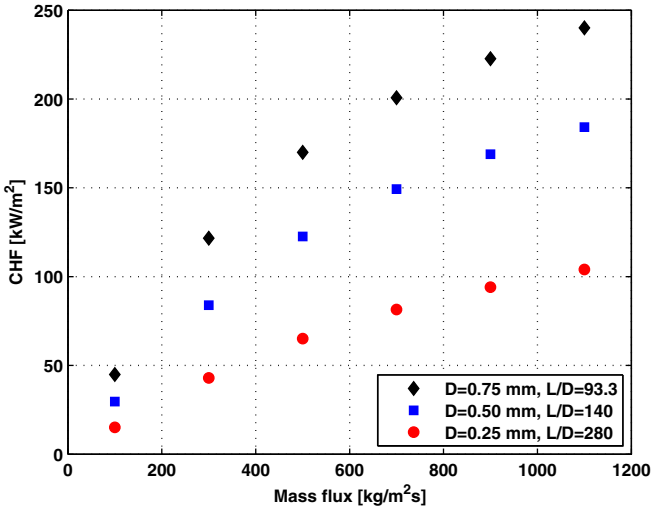

Fig. 13. Simulation of the influence of the mass flux G and the microchannel diameter D on the critical heat flux calculated with the current model for R-134a, $L = 70$ mm, $T_{sat} = 30$ °C and $\Delta T_{sub} = 0$ °C.

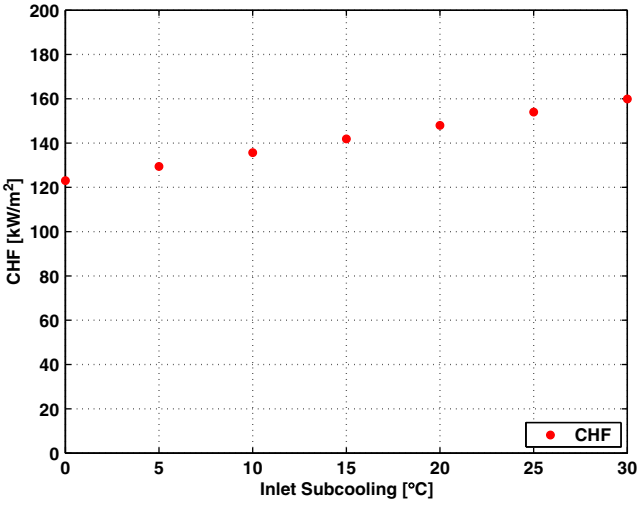

Fig. 15. Simulation of the influence of the inlet subcooling ΔT_{sub} on the critical heat flux calculated with the current model for R-134a, $D = 0.5$ mm, $L = 70$ mm, $T_{sat} = 30$ °C, $G = 500$ kg/m^2 s.

increases, the CHF increases as well. This diameter effect has been experimentally observed by Wojtan et al. [8]. These trends follow the well-known macroscale effect of L/D and G on CHF.

Fig. 14 presents a simulation of the variation of CHF with the heated length and the saturation temperature. As seen also experimentally, the shorter the heated length, the higher the CHF. Also, when the saturation temperature increases, CHF decreases.

Fig. 15 demonstrates that CHF is predicted to increase when increasing the inlet subcooling as expected, i.e. higher the inlet subcooling, the shorter is the two-phase zone. The influence is however limited, especially for low values of inlet subcooling.

6. Conclusions

A theoretical model for the prediction of the critical heat flux of saturated fluids flowing at stable conditions in heated, round microchannels has been developed. It is based on predicting the local dryout of the liquid film in annular flow occurring when the film thickness becomes equal to the interfacial wave height during evaporation. The model is based on the conservation of mass, momentum and energy, the Laplace–Young equation and a semi-empirical expression for the height of interfacial waves. Validation was carried out by comparing the model, that is a numerical solution of a non-linear system of five differential equations, with a database including three different refrigerants (R-134a, R-245fa and R-113) from two

different laboratories. More than 96% of the data were predicted within a ±20% error band and a mean absolute error of 8%. The inlet subcooling was also taken into account in the model. An advantage of the new model is its possible use with a non-uniform heat flux along microchannels cooling microprocessors. Furthermore, it was also possible to predict CHF data from a third laboratory for water and R-113 flowing in rectangular microchannels (using the width of the channel as the characteristic dimension) and in a test section with multiple circular microchannels. All together, 90% of the entire database including four different fluids and different geometries were predicted by the model within a ±20% error band and a mean absolute error of 9.3%.

Acknowledgements

R. Revellin is supported by the Swiss National Science Foundation (SFN) grant number 20 111626/1 on the topic of critical heat flux in microchannels.

References

[1] A.E. Bergles, S.G. Kandlikar, On the nature of critical heat flux in microchannels, J. Heat Transfer 127 (2005) 101–107.
[2] Y. Katto, H. Ohno, An improved version of the generalized correlation of critical heat flux for the forced convective boiling in uniformly heated vertical tubes, Int. J. Heat Mass Transfer 27 (9) (1984) 1641–1648.
[3] Y. Katto, S. Yokoya, CHF of forced convection boiling in uniformly heated vertical tubes, experimental study of hp-regime by the use of R12, Int. J. Multiphase Flow 8 (1982) 165–181.
[4] Y. Katto, S. Ashida, CHF in high pressure regime for forced convection boiling in uniformly heated vertical tube of low length-to-diameter-ratio, in: Proceedings 7th International Heat Transfer Conferences, vol. 4, 1982, pp. 291–296.
[5] Y. Katto, S. Yokoya, Critical heat flux of liquid helium (i) in forced convective boiling, Int. J. Multiphase Flow 10 (1984) 401–413.
[6] W. Qu, I. Mudawar, Measurement and correlation of critical heat flux in two-phase microchannel heat sinks, Int. J. Heat Mass Transfer 47 (2004) 2045–2059.
[7] M.B. Bowers, I. Mudawar, High flux boiling in low flow rate, low pressure drop mini-channel and micro-channel heat sinks, Int. J. Heat Mass Transfer 37 (1994) 321–332.
[8] L. Wojtan, R. Revellin, J. Thome, Investigation of critical heat flux in single, uniformly heated microchannels, Exp. Therm. Fluid Sci. 30 (2006) 765–774.
[9] R. Revellin, V. Dupont, T. Ursenbacher, J.R. Thome, I. Zun, Characterization of diabatic two-phase flows in microchannels: flow parameter results for R-134a in a 0.5 mm channel, Int. J. Multiphase Flow 32 (2006) 755–774.
[10] D.J. Pribyl, A. Bar-Cohen, A.E. Bergles, An investigation of critical heat flux and two-phase flow regimes for upward steam and water flow, in: Proceedings of the 5th International Conference in Boiling Heat Transfer, Jamaica, May 4–8, 2003.
[11] Y. Taitel, A.E. Dukler, A model for predicting flow regime transitions in horizontal and near horizontal gas–liquid flow, AIChE J. 22 (1) (1976) 47–55.
[12] L. Wojtan, T. Ursenbacher, J.R. Thome, Investigation of flow boiling in horizontal tubes: Part I – a new diabatic two-phase flow pattern map, Int. J. Heat Mass Transfer 48 (2005) 2955–2969.
[13] R. Revellin, J. Thome, New diabatic flow pattern map for evaporating flow in microchannels, in: 13th International Heat Transfer Conference, Sydney, Australia, 2006.
[14] R. Revellin, Experimental two-phase fluid flow in microchannels, Ph.D. thesis, Ecole polytechnique Fédérale de Lausanne, <http://library.epfl.ch/en/theses/?nr=3437> (2005).
[15] J.R. Thome, J.E. Hajal, A. Cavallini, Condensation in horizontal tubes, part 2: new heat transfer model based on flow regimes, Int. J. Heat Mass Transfer 46 (2003) 3365–3387.
[16] E. Kordyban, Some characteristics of high waves in closed channels approaching kelvin–helmholtz instability, J. Fluids Eng. 99 (1977) 346–389.
[17] G.M. Lazareck, S.H. Black, Evaporating heat transfer, pressure drop and critical heat flux in a small vertical tube with R-113, Int. J. Heat Mass Transfer 25 (7) (1982) 945–960.
[18] R. Revellin, J.R. Thome, Adiabatic two-phase frictional pressure drops in microchannels, Exp. Therm. Fluid Sci., in press.